Talanta 117 (2013) 133–138

Contents lists available at ScienceDirect

Talanta

journal homepage: www.elsevier.com/locate/talanta

Profiling differences in chemical composition of brain structures using Raman spectroscopy

Marko Daković [a,*], Aleksandra S. Stojiljković [a], Danica Bajuk-Bogdanović [a], Ana Starčević [b], Laslo Puškaš [b], Branislav Filipović [b], Snežana Uskoković-Marković [c], Ivanka Holclajtner-Antunović [a]

[a] Faculty of Physical Chemistry, Studentski trg 12-16, University of Belgrade, Belgrade, Serbia
[b] Institute of Anatomy Niko Miljanić, School of Medicine, Dr Subotića 4, University of Belgrade, Belgrade, Serbia
[c] Faculty of Pharmacy, Vojvode Stepe 450, University of Belgrade, Belgrade, Serbia

ARTICLE INFO

Article history:
Received 9 July 2013
Received in revised form
30 August 2013
Accepted 30 August 2013
Available online 6 September 2013

Keywords:
Raman spectroscopy
Brain tissue
Chemical composition
Independent component analysis

ABSTRACT

Raman spectroscopy enables non-invasive investigation of chemical composition of biological tissues. Due to similar chemical composition, the analysis of Raman spectra of brain structures and assignment of their spectral features to chemical constituents presents a particular challenge. In this study we demonstrate that standard and independent component analysis of Raman spectra is capable of assessment of differences in chemical composition between functionally related gray and white matter structures. Our results show the ability of Raman spectroscopy to successfully depict variation in chemical composition between structurally similar and/or functionally connected brain structures. The observed differences were attributed to variations in content of proteins and lipids in these structures. Independent component analysis enabled separation of contributions of major constituents in spectra and revealed spectral signatures of low-concentration metabolites. This provided finding of discrepancies between structures of striatum as well as between white matter structures. Raman spectroscopy can provide information about variations in contents of major chemical constituents in brain structures, while the application of independent component analysis performed on obtained spectra can help in revealing minute differences between closely related brain structures.

1. Introduction

Raman spectroscopy is a widely used method applied for qualitative, quantitative and structural analysis in chemical, biochemical and pharmaceutical research [1,2]. The ability for non-destructive or minimally destructive assessment of chemical composition and molecular interactions makes Raman spectroscopy suitable for *in vitro* as well as *in vivo* analysis of biological samples [3,4]. The application of this technique in assessment of compositional differences between normal and tissue affected by pathology provides information complementary to histological analysis [5,6]. So far, Raman spectroscopy has been applied in studies of normal brain tissue [7–9], detection and differentiation of various pathologies, including brain tumors [10–12], skin diseases [13,14], carcinoma of the neck [15], prostate [16] etc. However, the obtained spectra are very complex due to overlapping contributions of different molecular species which makes their analysis difficult.

The analysis and differentiation of Raman spectra of brain tissues presents a particular challenge due to their very similar chemical composition. Mizuno et al. established that spectra of gray and white matter essentially do not differ from those obtained from the rat brain [7]. They reported that dominant lines in Raman spectra arise from lipids and proteins, where contribution of the former is more pronounced in white matter. Sajid et al. [9] analyzed the intensity ratio of stretching vibrations in CH_2 and CH_3 groups (I_{CH2}/I_{CH3}) and found that the value of this parameter is lower in gray matter, indicating higher protein content [9]. Santos et al. used a single optic probe to acquire high wavenumber Raman spectra (2700–3100 cm^{-1}) of several structures present in coronal sections of the porcine brain [17]. They reported almost complete distinguishing of structures based on hierarchical cluster analysis of obtained spectra. Wolthuis et al. demonstrated that Raman spectroscopy can be a powerful tool for accurate determination of water concentration in the brain [18]. A number of studies dealt with spectra based distinguishing of normal brain tissue and tumors arising from brain parenchymal cells. However, to our

* Corresponding author. Tel.: +381112630796; Mob.: +381611147410.
E-mail address: marko@ffh.bg.ac.rs (M. Daković).

0039-9140/$ - see front matter © 2013 Elsevier B.V. All rights reserved.
http://dx.doi.org/10.1016/j.talanta.2013.08.058

knowledge there have been no studies dealing with Raman spectroscopy of structures which belong to human white and gray matter and reveal the spectral and compositional differences between them.

In this study, we demonstrate the ability of Raman spectroscopy to distinguish human gray matter structures: caudate nucleus (CN), putamen (PT) and cerebellar gray matter (CLG) as well as white matter structures: corticospinal tract (CST), pons (PN) and *septum pellucidum* (SP). We show that spectra provide the ability to reveal differences in the chemical composition of these structures using the classical approach classical approach (analysis of spectral line intensities) and the method of independent component analysis (ICA).

2. Materials and methods

2.1. Sample preparation

Specimens of deep gray matter (caudate nucleus and basal nuclei), cerebral gray matter and white matter (pons, nerve tract) and *septum pellucidum* were obtained from the Collection of brain tissues of the Institute of Anatomy of the School of Medicine, Belgrade. All samples in the collection were taken from a single cadaver (Program of Body Donation for Medical Research, Institute of Anatomy, Belgrade) within 6 h after death, kept in liquid nitrogen for two hours and stored at −80 °C. Half an hour before cutting, the specimens were transferred to a refrigerator at −20 °C. Ten consecutive 25 μm thick sections were cut (Leica Cryocut 1800) from specimens and transferred to microscopic plates. Prior to acquisition of Raman spectra, which was performed within 3 h after slicing, preparations were kept at −20 °C.

2.2. Raman instrumentation and spectra acquisition

Micro-Raman spectra of specimens were recorded in situ on a DXR Raman Microscope (Termo Scientific). The 532 nm line of a diode-pumped solid state high brightness laser was used as the exciting radiation and the power of illumination at the sample surface was 10 mW. Collection of the scattered light was made through an Olympus microscope with infinity corrected confocal optics, 25 μm pinhole aperture, standard working distance objective 50×, grating of 1800 lines/mm and resolution of 2 cm^{-1}. Acquisition time was 15 s with 10 scans. The laser spot diameter on the sample was 1 μm. Thermo Scientific OMNIC software was used for spectra collection and manipulation. For each of the specimens 10 Raman spectra were collected in the fingerprint region 600–1800 cm^{-1}. All spectra of each tissue were recorded from different spots within the same small area of a corresponding tissue specimen, so that tissue inhomogeneity effects could be minimized. None or slight degradation of samples was observed during experiments.

2.3. Analysis of Raman spectra

K-means cluster analysis (KMCA) (SPPS v 13) was performed on raw spectra obtained from a particular tissue in order to diminish the influence of surface heterogeneities which can be the source of errors in separation of components by ICA. The final number of clusters was set to be 2 and 100 iterations were performed. A cluster which contained a higher number of spectra was considered representative and served as input in the preprocessing step.

Raman spectra were preprocessed using Matlab® 2010a based package "Raman processing" [19]. Steps included application of a median filter in order to reduce noise in spectra, followed by subtraction of fluorescence and normalization of the spectrum by subtraction of minimal and then dividing by maximal intensity value. After these procedures intensities in spectra were in the range 0–1. Difference spectra were calculated for all tissue combinations in order to trace differences in content of major constituents (lipids and proteins).

2.4. Independent component analysis of Raman spectra

Independent component analysis is a statistical technique that extracts the source signals from a data matrix of multisensor recordings without *a priori* knowledge of constituents in analyzed samples [20]. The obtained data (x) can be represented as a linear combination of mutually independent components (s):

$$x_i = a_{i1}s_1 + a_{i2}s_2 + \cdots a_{in}s_n \text{ for all } i \quad (1)$$

where a_{in} represents abundance of the n-th component in a complex signal. It is more convenient to use vector matrix notation instead of sums used in the previous equation. Complex signal and independent components can be represented in the form of row vectors $\boldsymbol{x}=[x_1\ x_2 \ldots x_j]$ and $\boldsymbol{s}=[s_1\ s_2 \ldots s_n]$, while coefficients a_{ni} form mixing matrix **A**:

$$\mathbf{x} = \mathbf{A}\mathbf{s} \quad (2)$$

The problem of finding independent components is confined to obtaining the unmixing matrix **W** which satisfies equation

$$\mathbf{s} = \mathbf{W}\mathbf{x} \quad (3)$$

There are several different approaches for estimation of independent components. The FastICA algorithm uses the fixed-point iteration scheme for finding the maximum of non-Gaussianity of components, and the maxICA is based on maximizing of output entropy etc. The details of various techniques for ICA implementation can be found elsewhere [21,22].

Independent component analysis has been applied in analysis of various fields including medical image processing, analysis of recordings from electroencephalography (EEG), magnetoencephalography (MEG) [23,24], color decomposition of histologically stained samples etc. Spectroscopic data had been analyzed using this technique: it was successful in separation of signals of pure chemical compounds from their mixtures, obtaining spectra of major fractions in urine, etc. However, assignment of independent components to a particular chemical compound in spectra of human tissues cannot be achieved, which is a consequence of complex composition. Nevertheless, inspection of spectral features present in them may reveal signatures of constituents which were virtually absent or masked by other lines in original spectra.

Independent component analysis was performed in two steps using the FastICA toolbox [25] in Matlab 2010a and preprocessed spectra as input. First, principal component analysis (PCA) was performed in order to establish the major sources of variability in spectra and to achieve data reduction. Components whose sum of variances contributed with more than 99.0% to spectra were retained and whitened. In the second step the FastICA algorithm was performed using 10,000 iterations and fine tuning and the number of independent components was set to be equal to the number of retained principal components.

3. Results and discussion

3.1. Raman spectra of brain tissues

The average Raman spectra of gray (caudate nucleus, basal ganglia, cerebellar gray matter) and white matter structures (cerebral white matter, pons) as well as the *septum pellucidum* are given in Fig. 1. In all spectra the bands arising from contributions of lipids (1064, 1089, 1268, 1296, 1309, 1439 and 1659 cm^{-1}) [26],

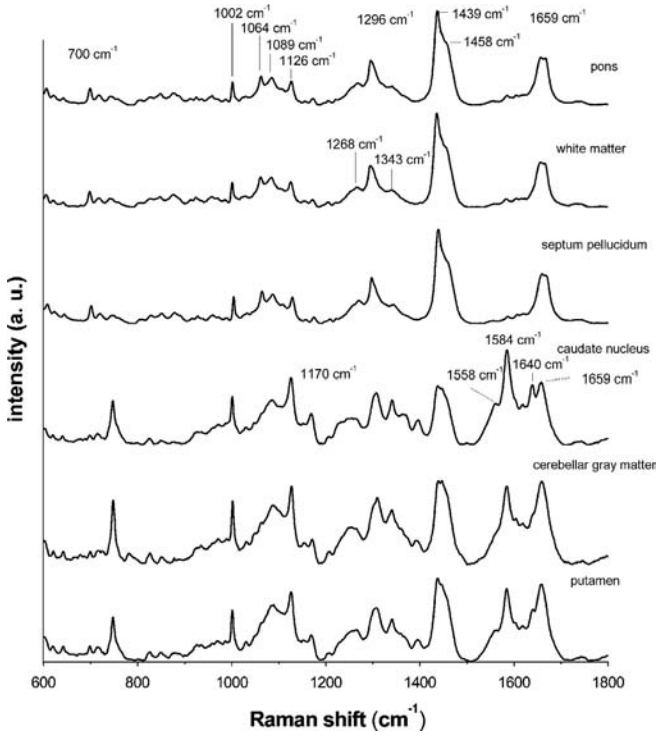

Fig. 1. Average Raman spectra of analyzed brain structures.

phenyl alanine residue in proteins (1002 cm^{-1}) and cholesterol (700 cm^{-1}) vibration modes are present. Bands at 1268 and 1659 cm^{-1} contain contributions from amide III and amide I bands in proteins. The detailed assignation of vibration bands observed in average Raman spectra is given in Table 1.

There are a few prominent differences between spectra of white and gray matter structures. The increased intensities of bands at 700, 720, 1268 and 1439 cm^{-1} pinpoint higher levels of cholesterol, sphingomyelin and saturated lipids in white matter structures. This is in agreement with findings of Krafft et al. who analyzed Raman spectra of lipid extracts of brain tissues [27]. They suggested that elevated intensity of bands from combined contributions of cholesterol and to a lesser extent from sphingomyelin originate from the presence of myelin in white matter. Studies dealing with chemical analysis of brain lipids gave the same conclusions [28]. The increased levels of saturated lipids in white matter are consistent with previous findings [29]. However, this does not imply different saturation of lipids in gray matter structures. Mizuno et al. reported that lipids in both white and gray matter exhibit similar chain lengths and the same degree of saturation [7].

On the other hand, in spectra of gray matter the increased intensities of bands at 1558, 1602, 1620, 1640 and 1659 cm^{-1} can be attributed to higher protein content. This is in agreement with findings of most of Raman spectroscopy studies of brain tissue [8,30,31] as well as findings of Banay-Schwartz et al. who analyzed protein composition of brain structures using the micro-punch technique [32]. The increased band intensity at 1659 cm^{-1} could be partly attributed to vibrations in the vinyl group of phospholipids and phosphatidyl choline whose content is higher in gray than in white matter [33]. The sharp Raman line at 1002 cm^{-1} suggests more frequent appearance of phenyl alanine residue in the protein sequence in gray matter. A high-intensity band at 747 cm^{-1}, which appears only in spectra of gray matter, arises from hemoglobin. This may be a consequence of the presence of high capillary density in gray matter.

Table 1
Assignment of vibration bands in Raman spectra of putamen, pons, cerebellar cortex, cerebral cortex, caudate nucleus and septum pelucidum. The data for assignation were taken from Movasaghi et al. [4].

Raman shift (cm^{-1})	Assignation
700	Cholesterol/sphygomyelin
720	Cholesterol/sphygomyelin
747	Hemoglobin
782	DNA, RNA bases
826	Proline/hydroxyproline
850	Proline, hydroxyproline, tyrosine
865	Ribose from RNA
922	Proline/hydroxyproline
1002	Phenyl alanine residue in proteins
1064	Skeletal C–C stretch of lipids
1089	ν(C–C) skeletal of acyl backbone in lipid
1126	Skeletal of acyl backbone in lipid, C-N stretching in proteins
1170	Tyrosine
1268	Triglycerides, fatty acids or amide III band of proteins
1296	CH_2 deformation band in lipid
1309	CH_3/CH_2 twisting or bending mode of lipid
1339	CH_2/CH_3 wagging, twisting &/or bending in lipids, nucleic acid modes
1374	DNA, RNA
1420	DNA, RNA
1439	CH2 deformation in lipids
1458	CH2/CH3 deformation of lipids & collagen
1485	DNA, RNA
1558	Tyrosine
1584	Pyrimidine ring (nucleic acids) & heme protein, phenyl alanine, tyrosine
1602	Phenylalanine
1608	Tyrosine, phenylalanine ring vibration
1620	Tryptophan
1640	Amide I band in proteins
1659	ν(C=C) cis, lipids, fatty acids and amide I band in proteins
1670	C=O in lipids

The obtained spectra of white matter structures contain a dominant contribution of vibrations in lipids. Due to the similarity of Raman spectra, SP was classified in this group. Protein bands are not easily observable (with the exception of phenyl alanine in proteins) which could be explained by masking of the dominant lipid contribution. Calculated differences between spectra of white matter structures (Fig. 2a and c) indicate higher band intensities (1064, 1126, 1296, and 1432 cm^{-1}), assigned to skeletal and deformation bands of lipid chains, in spectra of SP. This suggests the presence of higher levels of saturated lipids in this structure. The lower protein content in SP results in smaller intensity of proteins bands at 1659 and 1670 cm^{-1}. The difference spectrum for PN and CST (Fig. 2b) pinpoints higher levels of cholesterol/cholesterol ester (700 cm^{-1}) and unsaturated lipids in the former and higher content of saturated lipids in the latter. The increased density of nerve fibers and hence myelin content may be the cause of increased cholesterol in PN. Higher ratio of unsaturated/saturated lipids in this structure (which is more characteristic of gray matter) can be explained by the presence of gray matter islands (nuclei) in the bulk of white matter.

In the spectra of gray matter structures additional bands at 1126, 1558, 1602, 1620 and 1640 cm^{-1} can also be observed. They were assigned to C–N stretching vibration of proteins, tyrosine, tryptophan and amide I bands in proteins respectively. The last two correspond to the β-sheet, while the band at 1659 cm^{-1} contains a contribution of α-helix and random coil structure. However, determination of relative abundances of secondary structures in brain proteins is not reliable because of the presence of the lipid component. Nevertheless, the presence of a negative peak in the difference spectrum (Fig. 3a) for PT and CN suggests lower content of the β-sheet in the latter. Further, positive

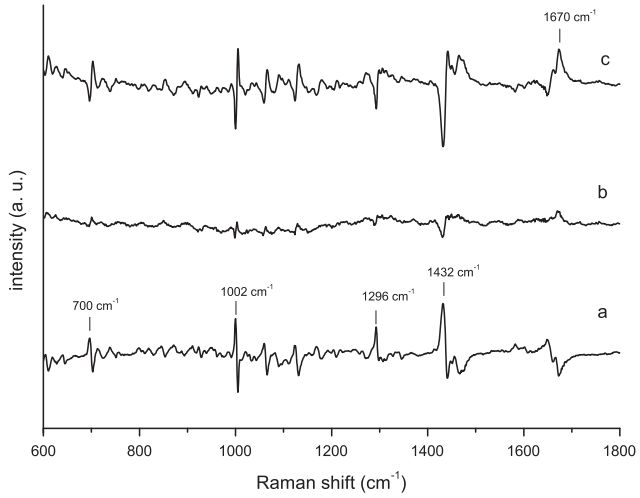

Fig. 2. Difference (subtraction) spectra for white matter structures: (a) pons–septum pelucidum, (b) pons–corticospinal tract, (c) septum–corticospinal tract.

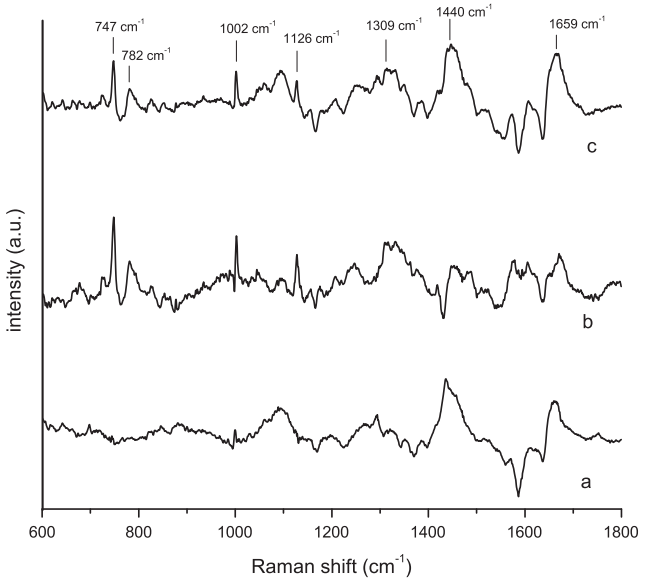

Fig. 3. Difference (subtraction) spectra for gray matter structures: (a) putamen–caudate nucleus, (b) putamen–cerebellar cortex, (c) caudate nucleus–cerebellar cortex.

peaks at 1659 and 1439 cm^{-1} can be attributed to a higher level of unsaturated and saturated lipids in PT. According to Mizuno et al. the relative contributions of lipids and proteins in spectra of brain structures can be determined by evaluation of intensity ratios of bands at 1439 and 1659 cm^{-1}[7]. We found that the lowest ratio ($I_{1439}/I_{1659}=0.92$) belonging to spectra of CN, could be explained by the presence of a denser aggregation of nerve cell bodies and hence lower lipid and/or higher protein content. Despite histological similarity and functional connections with CN, a different I_{1439}/I_{1659} ratio was found in spectra of PT (1.06). This may appear contradictory to the equal content of proteins in neostriatum structures [32]. The reason for this discrepancy may be in the fact that changes in band intensity at 1659 cm^{-1} cannot be an accurate measure of protein content due to the presence of the contribution of unsaturated lipids. The positive peaks in difference spectra at 1170, 1558 and 1585 cm^{-1} suggest an increased content of tyrosine and pyrimidine/purine bases in CN.

When compared to PT spectra, the increased intensities of bands at 747, 1002, 1126, 1558 and 1640 cm^{-1} in spectra of CLG suggest higher protein content (see Fig. 3b). Similar differences were observed between spectra of CN and CLG (Fig. 3c), with exceptions in region 1400–1650 cm^{-1} where more pronounced bands assigned to proteins and lower intensity bands assigned to lipids are noticed. Further, difference spectra suggest higher abundance of the β-sheet in the secondary structure of proteins (line at 1640 cm^{-1}) as well as higher levels of hemoglobin in cerebellar tissue. The latter can be explained by higher density of the capillary network in comparison to other gray matter structures. Further, spectra contain an additional band at 782 cm^{-1} which may be attributed to vibrations in nucleic acids.

It seems the elevation in intensities of lipid bands in spectra of gray matter follows the increase of glial cell numbers in series CLG, CN and PT. According to previous studies, it is the highest in CLG and the lowest in PT [34]. Considering the fact that oligodendrocytes comprise 75% of glial cells, variation of lipid levels could be largely attributed to variations in their number.

3.2. *Independent component analysis of Raman spectra of brain tissues*

The independent component analysis had separated Raman spectra of brain tissues in contributions which arise from different sources. All spectra of white matter structures can be adequately represented by two independent components where ICA 1 repeats for each of the analyzed structures (Fig. 4a–c). The common feature in this component is the exclusive presence of vibration bands arising from lipids. The distribution of spectral bands and their intensities are almost identical to Raman spectra of lipid extracts of human white matter reported by Kohler et al. [26]. However, a few differences between ICA 1 components for CST, PN and SP appear as change in intensity of bands at 1002 (phenyl alanine vibration), 1126, 1339 and 1659 cm^{-1} (Fig. 4). The last three arise from skeletal C–C, CH_2/CH_3 waging and CH_2/CH_3 deformation vibrations which appear at the same wavenumber for lipids and proteins. The differences in their intensity can be attributed to variation in protein content. The ICA 2 component in SP (Fig. 5a) differs significantly from corresponding components for other structures with only observable bands at 1002, 1439, 1659 cm^{-1} as well as a broad band at 1089 cm^{-1} which can be attributed to the stretch in PO_2^- groups of phospholipids. The abundance of this component, estimated from ICA is less than 0.5% which pinpoints to the highly homogeneous chemical composition of SP.

In the ICA 2 of CST and PN (Fig. 5b and c), the presence of protein as well as bands originating from combined contributions of lipids and proteins is noticeable. Since combined bands appear in both ICAs of white matter structures this suggests that lipid and protein contributions in them are separated. Further, ICA 2 for these structures is very similar, with the exception of the presence of weak bands which arise from nucleic acids at 865, 1094 and 1420 cm^{-1} in the white matter tract; they could not be observed in original spectra because of strong overlapping with lipid bands.

Spectra of gray matter structures can be adequately represented by three (CN and PT) and four (CLG) independent components which suggests higher compositional heterogeneity compared to white matter. When compared to white matter structures, similarity between ICA 1 components for PT and CN (Fig. 4d and e) and ICA 2 components in CST and PN (Fig. 5b and c) becomes apparent; the same holds for ICA 2 of former structures and ICA 1 of latter. This further confirms that independent component analysis of brain tissue could separate contributions from lipids and proteins. The most pronounced difference between CN and PT is observed in the region 1200–1300 cm^{-1} of ICA 2 components, which can be attributed to the amide band in proteins (see Fig. 5d and e). Beside phenyl alanine, bands which arise from amino acids proline (826 cm^{-1}), hydroxyproline (922 cm^{-1}) and tyrosine (1608 cm^{-1}) can be observed. The third

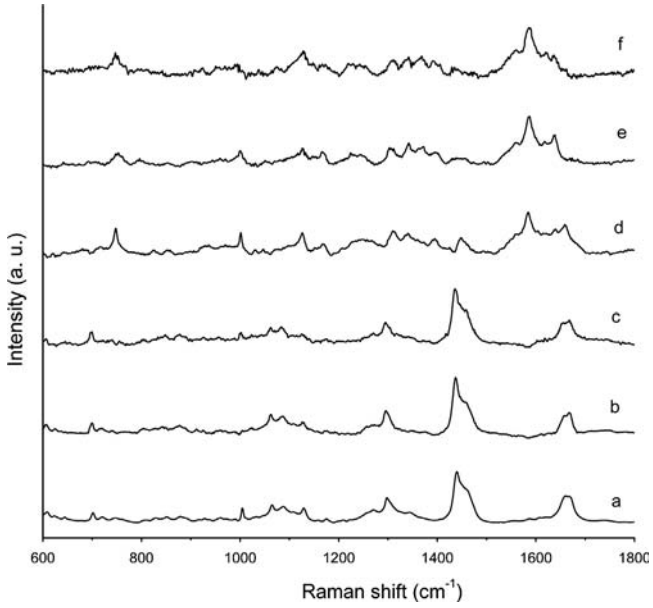

Fig. 4. The first independent components obtained for (a) septum, (b) pons, (c) corticospinal tract, (d) putamen, (e) caudate nucleus and (f) cerebellar cortex.

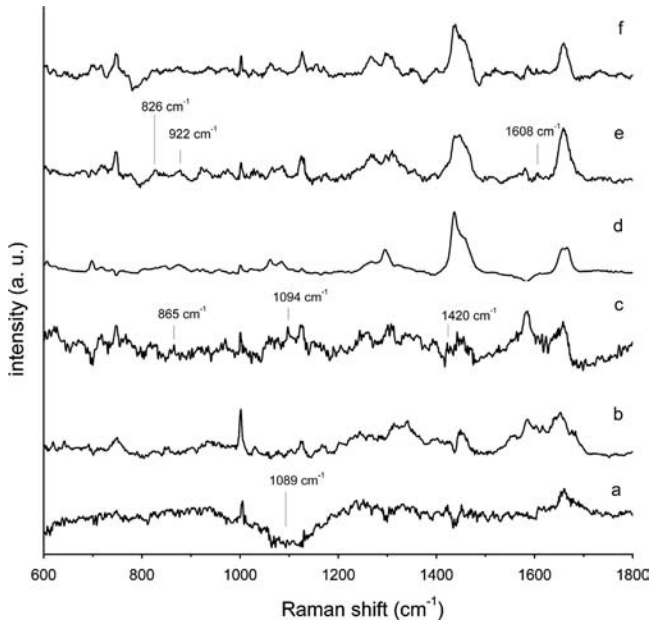

Fig. 5. The second independent components obtained for analyzed brain structures. For designation of spectra see fig. 4.

ICA in the CN and PT (Fig. 6d and e) is very similar to ICA 2 obtained from spectra of the *septum pellucidum* (see Fig. 5) which suggests their common origin. Lipid, protein and complex lipid–protein bands can be observed in these components.

Independent component analysis of CLG spectra gave four components with significant contributions. It can be noticed that ICA 1 (Fig. 4f) has a similar profile as ICA 3 in spectra of CN and putamen (Fig. 6d and e) and ICA 2 component in SP (Fig. 5a). The similarity can be also observed for ICA 2 components of CLG and SP. The ICA 3 (Fig. 6f) contains contributions of protein bands and combined lipid–protein bands. In the fourth ICA (Fig. 6g), beside amide I and III bands, vibrations of nucleotide bases from DNA and RNA at 782, 1094, 1248, 1374, 1420, 1485 and 1575 cm^{-1} become apparent. The appearance of these lines/bands in ICA 4 is probably

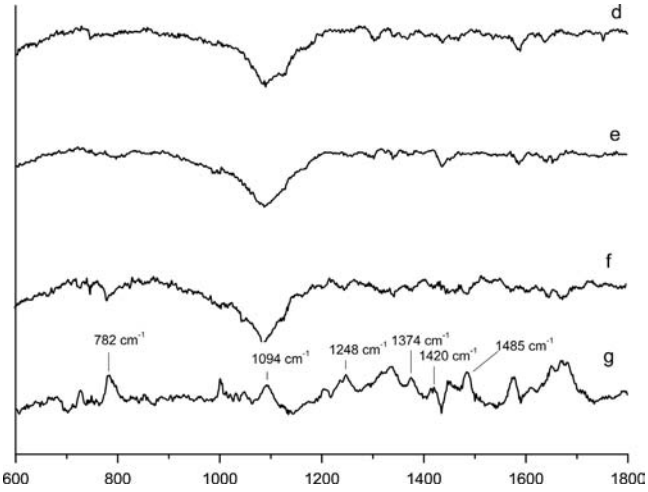

Fig. 6. The third independent components for putamen, caudate nucleus and cerebellar cortex ((d)–(f)) and the fourth ICA (g) for cerebellar cortex. Marked bands are assigned to contribution of nucleic acids.

a consequence of higher levels of nucleic acids compared with other brain structures.

Our results demonstrated the ability of Raman spectroscopy to successfully depict variation in chemical composition between structurally similar and/or functionally connected brain structures belonging to white and gray matter. Besides differences in content of major constituents (lipids and proteins), signs of different structural organization were also observed. This is particularly pronounced for gray matter where changes in the secondary structure of proteins as well as increased levels of unsaturated lipids were detected. Further, the difference spectra revealed variations in levels of some important amino acids. To our knowledge, this is the first time that Raman spectra of the human *septum pellucidum* had been recorded and evaluated. Tracing changes in this structure in neurological and psychiatric disorders was the subject of a number of morphological and histological studies. Raman spectroscopy could have added value in evaluation of compositional and structural changes in chemical constituents and could help in revealing those disease mechanisms.

The application of independent component analysis on Raman spectra led to separation of lipid and protein contributions which in turn enabled detection of spectral signatures of minor constituents like nucleic acids. Although the distribution of spectral bands and their intensities in a particular component may be almost identical to Raman spectra of constituents obtained by chemical extraction, due to the nature of ICA, only qualitative information from them can be considered reliable. Nevertheless, information obtained from an independent component enabled establishing minute differences between structures with similar phylogenetic origin and/or functional connections.

In this study PCA method was applied in preprocessing step for ICA, but not in spectra analysis. We gave advantage to ICA method in analysis of Raman spectra of brain tissues because the use of higher order statistics employed in this method provides more information about constituents of spectra and thus enables detection of latent differences in composition of tissues. Further, ICA resolves independent components in analyzed spectra, while PCA provides only their linear combinations which, frequently, are not physically interpretable. This enables more reliable assessment of contributions of constituents in common for lipid and protein spectral bands.

The fact that all samples originate from the same cadaver presents the major limitation in this study. Therefore no effects of age, sex and inter-subject variability were taken into account.

Evaluation of these factors on variations in spectra of brain tissues, especially gray matter structures will be the scope of forthcoming studies. Their results could provide new insight into changes of chemical composition in neurodegenerative diseases and hence help in understanding the mechanisms of their origination. The second shortcoming presents the random choice of regions in structures (punch-like sampling) from which spectra were obtained. Therefore the possible spectral variations in particular structures were neglected. The use of Raman mapping of some vibrations in their histological sections could help in solving this issue.

4. Conclusion

Raman spectroscopy provided assessment of compositional differences between white and gray matter structures, even in cases of existing structural similarity and/or functional connection. The obtained information about composition is complementary to those provided by standard chemical analysis of small elements of tissue sample. The minute differences between brain structures, which cannot be observed in original spectra, can be obtained by application of independent component analysis. Further, this technique enables separation of spectral contributions of main tissue constituents and provides insight in differences in their structure.

Acknowledgements

This study was supported by Grants No. III41005 and III41020 from the Ministry of Education, Science and Technological Development of the Republic of Serbia.

References

[1] P. Larkin, Infrared and Raman Spectroscopy; Principles and Spectral Interpretation, first ed., Elsevier, 2011.
[2] E. Smith, G. Dent, Modern Raman Spectroscopy: A Practical Approach, first ed., Wiley, 2005.
[3] M. Kirsch, G. Schackert, R. Salzer, C. Krafft, Anal. Bioanal. Chem. 398 (2010) 1707–1713.
[4] Z. Movasaghi, S. Rehman, I.U. Rehman, Appl. Spectrosc. Rev. 42 (2007) 493–541.
[5] E.Ó Faoláin, M.B. Hunter, J.M. Byrne, P. Kelehan, M. McNamara, H.J. Byrne, et al., Vib. Spectrosc. 38 (2005) 121–127.
[6] R. Rabah, R. Weber, G.K. Serhatkulu, A. Cao, H. Dai, A. Pandya, et al., J. Pediatr. Surg. 43 (2008) 171–176.
[7] A. Mizuno, H. Kitajima, K. Kawauchi, S. Muraishi, Y. Ozaki, J. Raman Spectrosc. 25 (1994) 25–29.
[8] A. Mizuno, T. Hayashi, K. Tashibu, S. Maraishi, K. Kawauchi, Y. Ozaki, Neurosci. Lett. 141 (1992) 47–52.
[9] J. Sajid, A. Elhaddaoui, S. Turrell, J. Raman Spectrosc. 28 (1997) 165–169.
[10] N. Amharref, A. Beljebbar, S. Dukic, L. Venteo, L. Schneider, M. Pluot, et al., Biochim. Biophys. Acta Biomembr 1768 (2007) 2605–2615.
[11] A. Beljebbar, S. Dukic, N. Amharref, M. Manfait, Anal. Bioanal. Chem. 398 (2010) 477–487.
[12] C. Krafft, S.B. Sobottka, G. Schackert, R. Salzer, J. Raman Spectrosc. 37 (2006) 367–375.
[13] S. Fendel, B. Schrader, Fresenius J. Anal. Chem. 360 (1998) 609–613.
[14] C.A. Lieber, S.K. Majumder, D. Billheimer, D.L. Ellis, A. Mahadevan-Jansen, Raman microspectroscopy for skin cancer detection in vitro, J. Biomed. Opt. 13 (2008) 024013.
[15] A.T. Harris, A. Rennie, H. Waqar-Uddin, S.R. Wheatley, S.K. Ghosh, D.P. Martin-Hirsch, et al., Head Neck Oncol 2 (2010) 26–31.
[16] P. Crow, B. Barrass, C. Kendall, M. Hart-Prieto, M. Wright, R. Persad, et al., Br. J. Cancer. 92 (2005) 2166–2170.
[17] L.F. Santos, R. Wolthuis, S. Koljenović, R.M. Almeida, G.J. Puppels, Anal. Chem. 77 (2005) 6747–6752.
[18] R. Wolthuis, A. van, K. Fountas, J.S. Robinson, H.A. Bruining, G.J. Puppels, Anal. Chem. 73 (2001) 3915–3920.
[19] L.A. Reisner, A. Cao, A.K. Pandya, Chemom. Intell. Lab. Syst 105 (2011) 83–90.
[20] A. Hyvärinen, E. Oja, Neural Netw 13 (2000) 411–430.
[21] D.J.-R. Bouveresse, H. Benabid, D.N. Rutledge, Anal. Chim. Acta. 589 (2007) 216–224.
[22] G. Wang, Q. Ding, Z. Hou, TrAC Trends Anal. Chem 27 (2008) 368–376.
[23] F. Esposito, T. Scarabino, A. Hyvarinen, J. Himberg, E. Formisano, S. Comani, et al., NeuroImage 25 (2005) 193–205.
[24] S. Makeig, T.P. Jung, A.J. Bell, D. Ghahremani, T.J. Sejnowski, Proc. Nat. Acad. Sci 94 (1997) 10979–10984.
[25] A. Hyvarinen, IEEE Trans 10 (1999) 626–634.
[26] M. Kohler, S. Machill, R. Salzer, C. Krafft, Anal. Bioanal. Chem. 393 (2009) 1513–1520.
[27] C. Krafft, L. Neudert, T. Simat, R. Salzer, Spectrochim. Acta. A. Mol. Biomol. Spectrosc 61 (2005) 1529–1535.
[28] A.C. Johnson, A.R. McNabb, R.J. Rossiter, Biochem. J. 44 (1949) 494.
[29] A.C. Johnson, A.R. McNabb, R.J. Rossiter, Biochem. J. 43 (1948) 573.
[30] C. Krafft, S.B. Sobottka, G. Schackert, R. Salzer, Analyst 130 (2005) 1070.
[31] C. Krafft, S.B. Sobottka, G. Schackert, R. Salzer, Analyst 129 (2004) 921.
[32] M. Banay-Schwartz, A. Kenessey, T. DeGuzman, A. Lajtha, M. Palkovits, Age 15 (1992) 51–54.
[33] S. Brady, G. Siegel, R.W. Albers, D. Price (Eds.), Basic Neurochemistry, seventh ed.; Molecular, Cellular and Medical Aspects, seventh ed.,Academic Press, 2005.
[34] F.A.C. Azevedo, L.R.B. Carvalho, L.T. Grinberg, J.M. Farfel, R.E.L. Ferretti, R.E. P. Leite, et al., J. Comp. Neurol. 513 (2009) 532–541.